PNAS RESEARCH ARTICLE | BIOCHEMISTRY

Potent monoclonal antibody–mediated neutralization of a divergent Hendra virus variant

Zhaoqian Wang[a,1], Ha V. Dang[a,1], Moushimi Amaya[b,c,1], Yan Xu[d,1], Randy Yin[b,c], Lianying Yan[b,c], Andrew C. Hickey[c,e], Edward J. Annand[f,g,h,i], Bethany A. Horsburgh[j,k], Peter A. Reid[l], Ina Smith[h], John-Sebastian Eden[j,k], Kai Xu[d,2], Christopher C. Broder[b,2], and David Veesler[a,m,2]

Edited by Benhur Lee, Icahn School of Medicine at Mount Sinai, New York, NY; received December 16, 2021; accepted April 16, 2022 by Editorial Board Member Adolfo Garcia-Sastre

Hendra virus (HeV) and Nipah virus (NiV) are deadly zoonotic *Henipaviruses* (HNVs) responsible for recurrent outbreaks in humans and domestic species of highly fatal (50 to 95%) disease. A HeV variant (HeV-g2) of unprecedented genetic divergence has been identified in two fatally diseased horses, and in two flying fox species in regions of Australia not previously considered at risk for HeV spillover. Given the HeV-g2 divergence from HeV while retaining equivalent pathogenicity and spillover potential, understanding receptor usage and antigenic properties is urgently required to guide One Health biosecurity. Here, we show that the HeV-g2 G glycoprotein shares a conserved receptor tropism with prototypic HeV and that a panel of monoclonal antibodies recognizing the G and F glycoproteins potently neutralizes HeV-g2– and HeV G/F–mediated entry into cells. We determined a crystal structure of the Fab fragment of the hAH1.3 antibody bound to the HeV G head domain, revealing an antigenic site associated with potent cross-neutralization of both HeV-g2 and HeV. Structure-guided formulation of a tetravalent monoclonal antibody (mAb) mixture, targeting four distinct G head antigenic sites, results in potent neutralization of HeV and HeV-g2 and delineates a path forward for implementing multivalent mAb combinations for postexposure treatment of HNV infections.

Hendra virus | Nipah virus | antibodies | variants | receptor

Hendra virus (HeV) and Nipah virus (NiV) are highly pathogenic viruses of the *Henipavirus* (HNV) genus in the *Paramyxoviridae* family, causing fatal diseases in various mammalian species including horses, pigs, and humans (1). HNVs are enveloped viruses and infect host cells through fusion of the viral and cell membranes. This process is mediated by the concerted action of two glycoproteins on the HNV surface known as G (attachment glycoprotein) and F (fusion glycoprotein). HNV G, also known as the receptor-binding protein, is homotetrameric with an N-terminal transmembrane domain followed by a stalk domain and a C-terminal head domain (2), the latter recognizing ephrin-B2 (EB2) and ephrin-B3 (EB3) as entry receptors (3–7). F is a homotrimeric class I viral fusion protein, processed by host cathepsin L in the endosomal compartment via a recycling process (8–10). Both G and F are required for HNV infection and are the targets of the neutralizing humoral immune response (2, 11–14). Serum neutralizing antibodies against F and G are a correlate of protection in animals experimentally infected with NiV or HeV (15–18).

F and G are the basis for the design and development of candidate postexposure therapies and vaccines against HNVs (19). A licensed horse subunit vaccine (Equivac HeV) based on the HeV G protein ectodomain (sG) has been used in Australia since 2012 (20). A HeV sG-based human vaccine is also currently being evaluated in a phase 1 clinical trial (21). Several anti-F and anti-G monoclonal antibodies (mAbs) have been identified and shown to have potent neutralizing activity against both NiV and HeV (2, 11, 12, 14, 22–24). The G-specific m102.4 mAb has been administered to 16 individuals as an emergency postexposure therapy on a compassionate basis and has demonstrated desirable safety and immunogenicity properties in a phase 1 clinical trial (25).

A novel Hendra virus variant (HeV-g2) was detected in Australia in horses that succumbed to fatal HeV illness and in two species of flying foxes suffering vasculitis (26, 27). Despite frequent HeV testing in horses in areas with known viral circulation in wildlife, this new HeV-g2 escaped routine PCR-based testing due to much lower sequence conservation than ever detected compared with prototypic HeV. Furthermore, HeV-g2 was detected in regions of Australia previously thought to be at low risk of HeV cross-species transmission (26, 27). HeV-g2 F and G share 95.60 and 92.85% amino acid sequence identity with their counterparts in prototypic HeV, respectively.

Significance

A new Hendra virus variant (HeV-g2) has been recently identified in two independent studies, increasing the concern of HeV spillover. Here, we show that HeV-g2 utilizes the same host receptor as HeV and that a panel of previously described HeV neutralizing antibodies cross-neutralizes HeV-g2 potently. Furthermore, we describe a monoclonal antibody (hAH1.3) neutralizing HeV and HeV-g2 and reveal its epitope using X-ray crystallography. We show that targeting four nonoverlapping epitopes on the HeV attachment protein simultaneously leads to potent HeV and HeV-g2 neutralization, supporting the development of a tetravalent monoclonal antibody cocktail. Collectively, our data provide a comprehensive assessment of available countermeasures against this newly described HeV-g2 variant and delineate multiple strategies for pandemic preparedness.

This article is a PNAS Direct Submission. B.L. is a guest editor invited by the Editorial Board.

[1]Z.W., H.V.D., M.A., and Y.X. contributed equally to this work.

[2]To whom correspondence may be addressed. Email: xu.4692@osu.edu, christopher.broder@usuhs.edu, or dveesler@uw.edu.

This article contains supporting information online at http://www.pnas.org/lookup/suppl/doi:10.1073/pnas.2122769119/-/DCSupplemental.

Published May 26, 2022.

Given the marked genetic divergence of HeV-g2 relative to HeV, it is unknown whether this newly discovered virus will share similar receptor usage and antigenic properties relative to prototypic HeV. Here, we set out to investigate the ability of HeV-g2 to utilize EB2 and EB3 as receptors for entry into cells and the likelihood that postexposure therapies and vaccines in development will be effective against this new variant. Here, we show that several HNV F- and G-specific mAbs cross-react with HeV-g2 glycoproteins and inhibit entry into target cells. We identify and characterize a mAb cross-neutralizing HeV and HeV-g2, designated hAH1.3, and determined its structure bound to the HeV G head domain, revealing recognition of an antigenic site distinct from those targeted by all other known HNV G-reactive mAbs. These data delineate a path forward to deploy mAb mixtures with a high barrier to the emergence of escape mutants.

Results

HeV-g2 and HeV Share a Conserved Receptor Tropism. Comparison of the HeV and HeV-g2 G sequences revealed that there are 33 residue substitutions between the two variants, most of them clustering within the receptor-binding G head domain (*SI Appendix*, Fig. S1). To understand the effect of these substitutions on receptor usage, we evaluated binding of purified monomeric HeV and HeV-g2 G head domains to immobilized EB2 and EB3 genetically fused to the human immunoglobulin 1 (IgG1) Fc fragment using biolayer interferometry (BLI). Despite the four residue differences between human EB2 (hEB2) and *Pteropus alecto* EB2 (PaEB2), both G head domain variants bound indistinguishably with monovalent binding affinities in the 0.5 to 1 nM range (Fig. 1 *A*, *B*, *D*, and *E* and *SI Appendix*, Fig. S2 *A–D*). The strictly conserved EB3 bound with comparable affinities to HeV and HeV-g2 G head domains, though affinities for EB3 were much lower than for EB2 (Fig. 1 *A*, *C*, *F*, and *G* and *SI Appendix*, Fig. S2 *E–H*). These findings suggest that HeV-g2 recognizes each of the two known human receptor subtypes with similar efficiency to HeV, consistent with the strict conservation of the receptor-binding interface. Furthermore, the small number of (largely conservative) mutations found between hEB2 and PaEB2 and the strict conservation of hEB3 and PaEB3 (*SI Appendix*, Fig. S2) concur with the undistinguishable binding properties observed here across orthologs, supporting the role of flying foxes as reservoir hosts for both variants of HeV (and NiV).

To investigate the ability of HeV-g2 to utilize hEB2 and hEB3 for cell entry, we generated a green fluorescent protein (GFP)–encoding, replication-competent, Cedar (henipa)virus (rCedV) chimera in which the native glycoproteins are substituted with the HeV-g2 F and G glycoproteins (rCedV-HeV-g2-GFP). Stable expression of hEB2 (HeLa-USU-EB2) or hEB3 (HeLa-USU-EB3) rendered HeLa-USU cells susceptible to rCedV-HeV-g2-GFP, as was the case for the rCedV-HeV-GFP positive control which harbors the prototypical HeV F and G glycoproteins

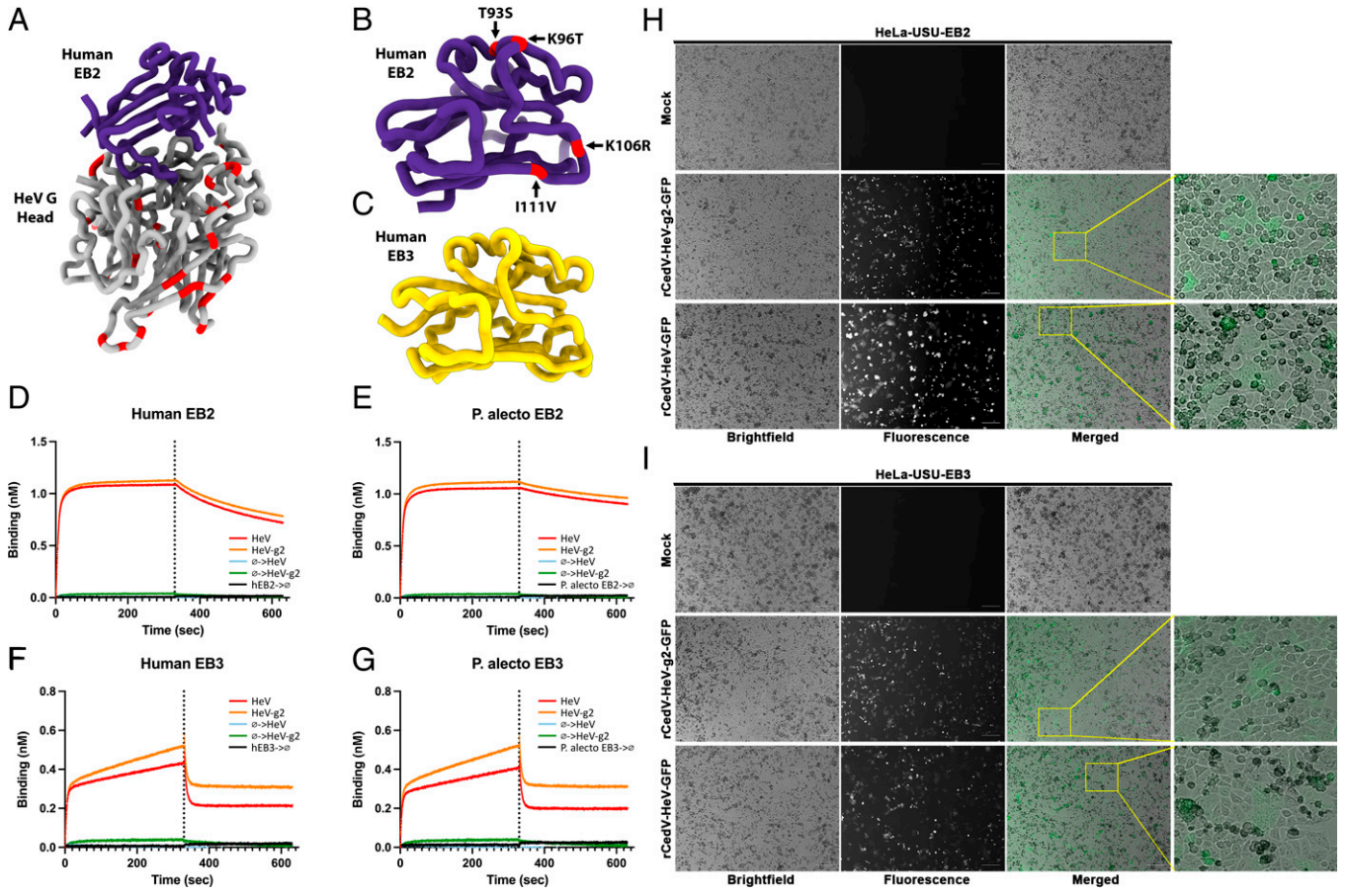

Fig. 1. HeV and HeV-g2 share a conserved receptor tropism. (*A*) Ribbon diagram of a HeV G head domain (gray) in complex with human EB2 (purple). Residues mutated between the HeV G and HeV-g2 G head domains are colored red. The rendering was made using PDB ID code 6PDL. (*B* and *C*) Ribbon diagram of human EB2 (*B*; PDB ID code 6PDL) and EB3 (*C*; PDB ID code 3D12). Residues that differ between human and *P. alecto* orthologs are colored red. (*D–G*) BLI binding analysis of 200 nm HeV (red) or HeV-g2 (orange) G head domain to immobilized human EB2-Fc (*D*), *P. alecto* EB2-Fc (*E*), human EB3-Fc (*F*), or *P. alecto* EB3-Fc (*G*). All ephrin-Fc fusions were immobilized on AHC biosensors. (*H* and *I*) EB2 and EB3 are entry receptors for rCedV-HeV-g2-GFP. (Scale bars, 50 μm.) (*H* and *I*, *Insets*) Zoomed-in regions within the yellow boxes. Bright-field, fluorescence, and merged images are shown (*Left* to *Right*).

(Fig. 1 *H* and *I* and *SI Appendix*, Fig. S3) (7, 28–30). We did not observe any significant differences in the percentage of GFP foci upon rCedV-HeV-g2-GFP infection of HeLa-USU-EB2 (91%) or HeLa-USU-EB3 (98%) cells compared with rCedV-HeV-GFP (set to 100%). No evidence of infection was observed in HeLa cells infected with either rCedV-HeV-g2-GFP or rCedV-HeV-GFP (*SI Appendix*, Fig. S3). Therefore, HeV-g2 retains the same receptor tropism as HeV and is expected to have a similar tissue tropism upon infection of humans and other animals.

Broadly Neutralizing HNV F-Specific mAbs Inhibit HeV-g2. We previously described and humanized a panel of F-specific mouse mAbs, designated 1F5, 5B3, and 12B2, binding to two distinct, prefusion-specific quaternary antigenic sites and broadly neutralizing NiV and HeV by blocking membrane fusion (11, 12). Therapeutic administration (up to several days after infection) of a humanized 5B3 derivative protected ferrets challenged with lethal doses of NiV or HeV (18), underscoring the importance of F-specific mAbs for treatment of NiV and HeV infections.

The HeV-g2 F glycoprotein differs from HeV F at 25 out of a total of 546 amino acid residues, with 10 substitutions mapping to the predicted signal peptide (residues 1 to 26) (*SI Appendix*, Fig. S1). To understand the impact on antigenicity of the sequence divergence across HeV-g2 and HeV F glycoproteins, we compared binding of the 1F5, 5B3, and 12B2 mAbs to prefusion-stabilized HeV-g2 and HeV F ectodomain trimers. All three mAbs cross-reacted with identical binding kinetics and affinities with the two variant virus F trimers, consistent with the mutations mapping outside of the antigenic sites recognized by these mAbs, except for the $S_{HeV}/T_{NiV}81N_{HeV\text{-}g2}$ substitution, which is at the periphery of the 1F5/5B3 epitopes and does not interfere with binding (Fig. 2 *A*–*F* and

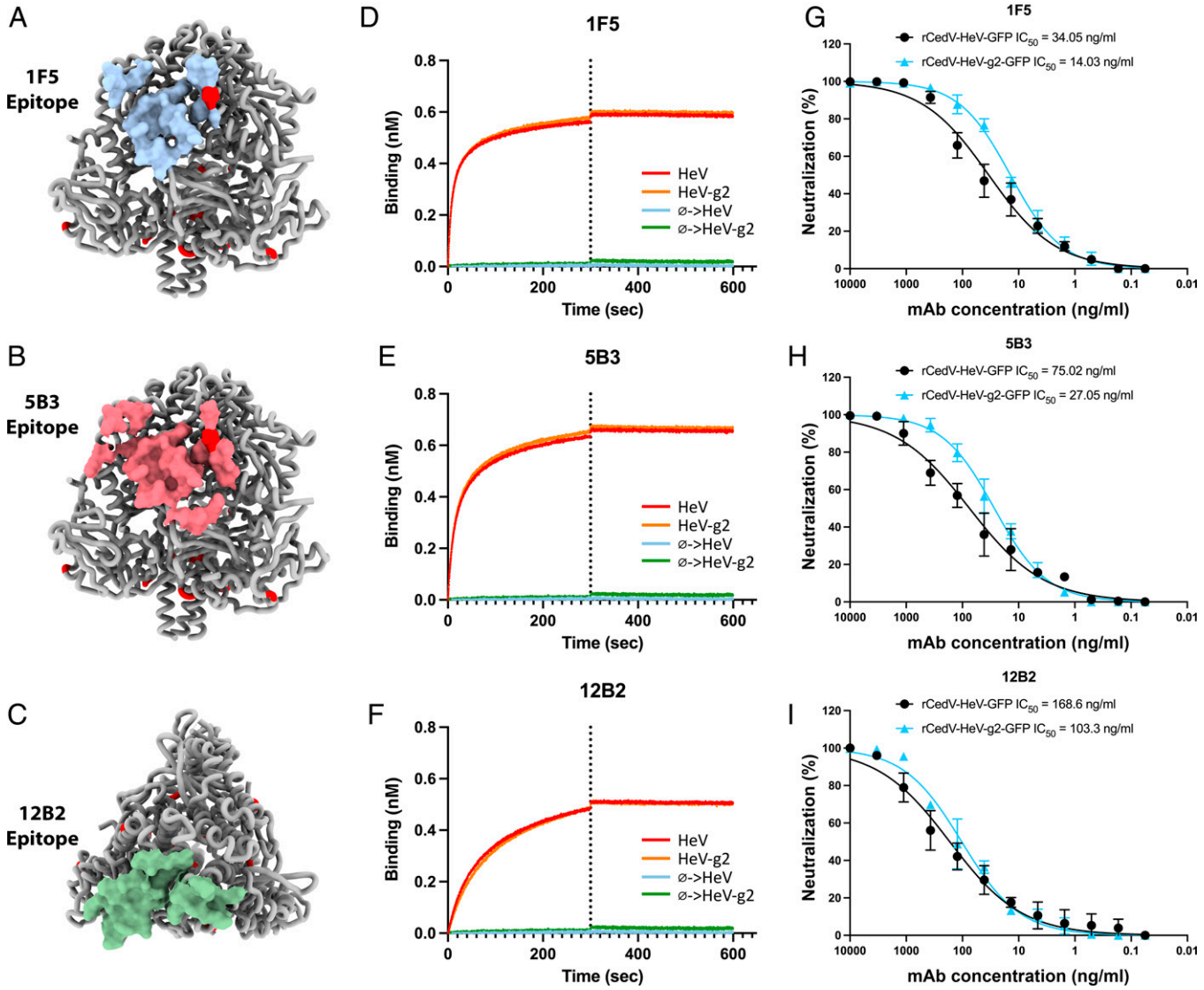

Fig. 2. Broadly neutralizing HNV F-specific mAbs inhibit HeV-g2. (*A*–*C*) Ribbon diagram of HeV F (PDB ID code 7KI6) ectodomain (gray) with the 1F5-interacting surface (blue), 5B3-interacting surface (red), or 12B2-interacting surface (green) highlighted. Residues that are mutated in HeV-g2 F relative to HeV F are colored red. *A* and *B* correspond to views along the plane of the viral membrane (F viewed from the side) whereas *C* corresponds to a view normal to and looking toward the viral membrane (F viewed from the top). (*D*–*F*) BLI binding analysis of 300 nm HeV (red) or HeV-g2 (orange) F ectodomain trimer to 1F5 IgG (*D*), 5B3 IgG (*E*), or 12B2 IgG (*F*) immobilized at the surface of AMC biosensors. (*G*–*I*) 1F5- (*G*), 5B3- (*H*), and 12B2-mediated (*I*) neutralization of rCedV-HeV-GFP (black) or rCedV-HeV-g2-GFP (blue). The limit of detection for the neutralization assay was 50 fluorescent foci. The differences of IC_{50} values for each mAb between rCedV-HeV-GFP and rCedV-HeV-g2-GFP were not statistically significant (Student's *t* test) with *P* values of 0.110, 0.255, and 0.333 for 1F5, 5B3, and 12B2, respectively. Error bars: SD. Moreover, we observed Pearson correlations of 0.9732, 0.9718, and 0.9897 for the 1F5, 5B3, and 12B2 IC_{50} values, respectively, between rCedV-HeV-GFP and rCedV-HeV-g2-GFP with *P* values smaller than 0.0001.

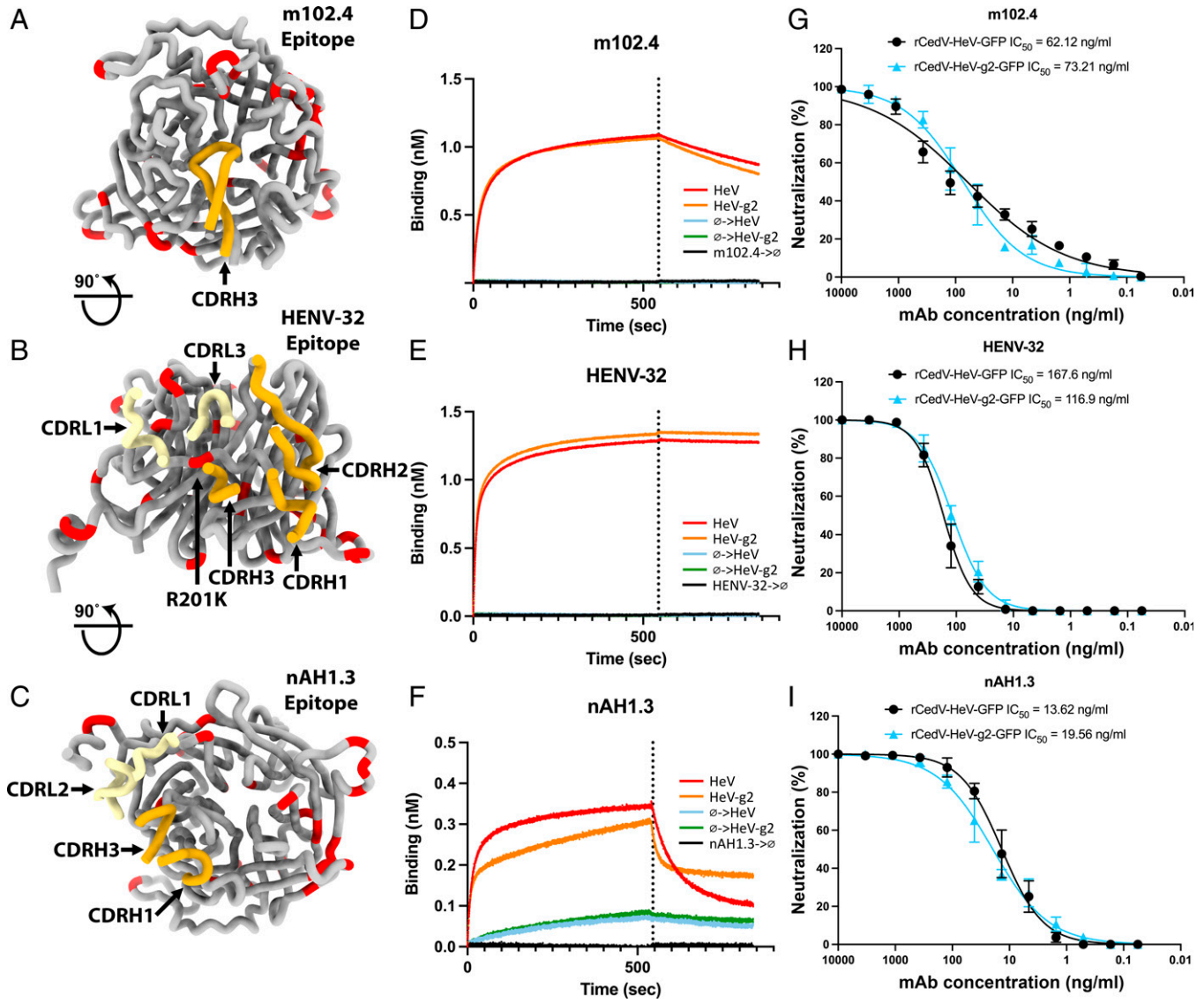

Fig. 3. Broadly neutralizing HNV G-specific mAbs inhibit HeV-g2. (*A–C*) Ribbon diagram of the HeV G head domain (gray) with the interacting heavy- and light-chain complementarity-determining regions (CDRs) of m102.3 (parent mAb of m102.4; PDB ID code 6CMI) (*A*), HENV-32 (PDB ID code 6VY4) (*B*), and nAH1.3 (PDB ID code 7TXZ) (*C*) rendered in gold and yellow, respectively. Residues that are mutated in HeV-g2 G relative to HeV G are colored red. (*D–F*) BLI binding analysis of 100 nm HeV (red) or HeV-g2 (orange) G head domain to m102.4 (*D*), HENV-32 (*E*), or nAH1.3 (*F*) IgG immobilized at the surface of AHC biosensors. (*G–I*) m102.4- (*G*), HENV-32– (*H*), and nAH1.3-mediated (*I*) neutralization of rCedV-HeV-GFP (black) or rCedV-HeV-g2-GFP (blue). The limit of detection for the neutralization assay was 50 fluorescent foci. The differences of IC_{50} values for each mAb between rCedV-HeV-GFP and rCedV-HeV-g2-GFP were not statistically significant (Student's *t* test) with *P* values of 0.447, 0.609, and 0.117 for m102.4, HENV-32, and nAH1.3, respectively. Error bars: SD. Moreover, we observed Pearson correlations of 0.9819, 0.9942, and 0.9909 for the m102.4, HENV-32, and nAH1.3 IC_{50} values, respectively, between rCedV-HeV-GFP and rCedV-HeV-g2-GFP with *P* values smaller than 0.0001.

SI Appendix, Fig. S4 and Table S1). Side-by-side comparison of mAb-mediated neutralization of rCedV-HeV-g2-GFP and rCedV-HeV-GFP showed that 1F5, 5B3, and 12B2 inhibited viral entry with virtually identical potencies against each of the two variants (Fig. 2 *G–I* and *SI Appendix*, Table S2). Our results demonstrate that these three F-specific broadly neutralizing HNV mAbs potently inhibit HeV-g2 and are resilient to the HeV and NiV genetic diversity sampled thus far.

Broadly Neutralizing HNV G-Specific mAbs Inhibit HeV-g2. Several G-targeted neutralizing mAbs have been described and shown to protect against lethal HeV and NiV challenge in a postexposure setting (2, 13, 16, 17, 23, 24, 31). Here, we investigated whether three potent and noncompeting neutralizing mAbs, m102.4, HENV-32, and nAH1.3, can cross-react with HeV-g2 G and neutralize rCedV-HeV-g2-GFP. Only 1 out of 33 residues that are mutated between HeV-g2 and prototypic HeV maps to an epitope recognized by one of these mAbs: The conservative R201K substitution is found within the HENV-32 binding site and recapitulates the NiV G K201 residue, explaining that HENV-32 broadly neutralizes NiV, HeV, and HeV-g2 (23) (Fig. 3 *A–C*). Indeed, we found that m102.4 and HENV-32 bound to each variant indistinguishably whereas nAH1.3 recognized the two variants with roughly comparable efficiencies by BLI (Fig. 3 *D–F*). Enzyme-linked immunosorbent assays (ELISAs) also indicated that each mAb has comparable affinity for the HeV and HeV-g2 G head domains, including the neutralizing mAbs HENV-103 and HENV-117 (*SI Appendix*, Fig. S5) (24). The neutralization potency of m102.4, HENV-32, and nAH1.3 was comparable against each of the two viruses (rCedV-HeV-g2-GFP and rCedV-HeV-GFP) with nAH1.3 exhibiting an order of magnitude greater neutralizing activity

than the other two mAbs (Fig. 3 *G–I*). These data show that broadly neutralizing HNV mAbs recognizing three distinct G head domain antigenic sites are potent inhibitors of the recently described HeV-g2 variant.

The hAH1.3 Neutralizing mAb Defines a HeV/HeV-g2 G Antigenic Site. The mouse hAH1.3 mAb was previously reported to potently neutralize HeV but not NiV (31). We determined a crystal structure of the hAH1.3 Fab fragment in complex with the HeV G head domain at 2.75-Å resolution (*SI Appendix*, Table S4). hAH1.3 interacts with an antigenic site located opposite of the head–head dimerization interface and thus of the HENV-32 epitope (23), which is also distinct from the receptor binding site (4, 6) or the nAH1.3 epitope (2) (Fig. 4*A*). As a result, hAH1.3 does not compete with the hEB2 receptor for binding to the HeV G head domain (as opposed to m102.4) and is unlikely to disturb the G head–head dimerization interface (in contrast to HENV-32) (Fig. 4*A* and *SI Appendix*, Fig. S6). hAH1.3 binding does not induce major conformational changes of the HeV G head domain. All six hAH1.3 complementary determining regions participate in the paratope through shape complementarity and hydrogen bonding burying an excess of 1,000 Å^2 at the interface with HeV G and involving contacts with the HeV G polypeptide and N-linked oligosaccharides at positions N378, N481, and N529 (Fig. 4*B* and *SI Appendix*, Figs. S7 and S8). The sole residue substitution in the hAH1.3 epitope ($H_{HeV}386N_{HeV\text{-}g2}$) does not prevent cross-reactivity with both HeV and HeV-g2 head domains, as observed using BLI (Fig. 4 *C* and *D* and *SI Appendix*, Fig. S1 and Table S2). Accordingly, hAH1.3 inhibited with comparable potencies rCedV-HeV-GFP (50% inhibitory concentration [IC_{50}]: 25.47 ng/mL) and rCedV-HeV-g2-GFP (IC_{50}: 22.07 ng/mL) (Fig. 4*E*). Although the structure suggests that the effect of individual NiV G substitutions within the hAH1.3 epitope relative to HeV G (I385T, H386K, K388Q, and S483T) is expected to be moderate, the additive effect of all four mutations likely explains the lack of hAH1.3 cross-reactivity with NiV (Fig. 4 *C* and *F* and *SI Appendix*, Fig. S1).

Structure-Guided Formulation of a Tetravalent mAb Mixture. Superimposition of the m102.4-, HENV-32–, nAH1.3-, and hAH1.3-bound G structures indicated that the four mAbs target entirely distinct, nonoverlapping antigenic sites on HNV G (Fig. 5*A*). Using BLI, we confirmed that all four mAbs can simultaneously recognize the HeV or HeV-g2 G head domain immobilized at the surface of biosensors upon sequential incubation with combinations of these mAbs (Fig. 5*B*). Furthermore, an equimolar mixture of all four mAbs mediated potent, concentration-dependent inhibition of both rCedV-HeV-GFP and rCedV-HeV-g2-GFP (Fig. 5*C*). Given that HENV-32 recognizes an antigenic site buried at the interface between G protomers and based on steric considerations, it is possible that binding of the four-mAb mixture would disrupt G tetramers, as observed with some coronavirus mAbs (32–37), possibly contributing to neutralization. These data delineate a path forward for deploying multivalent mAb combinations for postexposure treatment that would pose a higher barrier to the emergence of escape mutants than individual constituting mAbs (2).

To further evaluate the possible effects of the HeV-g2 G amino acid sequence variation on its antigenic landscape, we measured the neutralizing activity of rhesus macaque polyclonal sera elicited by immunization with equimolar concentrations of NiV-Malaysia sG and NiV-Bangladesh sG (2). We determined serum neutralizing activities of 1/578 and 1/894 against rCedV-HeV-GFP and rCedV-HeV-g2-GFP, respectively, for one animal, and of 1/242 and 1/714 against rCedV-HeV-GFP and rCedV-HeV-g2-GFP, respectively, for the second animal (Fig. 5 *D–F*). In both cases, the sera are slightly more potent against HeV-g2 than HeV (vaccine-mismatched) but less than NiV (vaccine-matched), for which the neutralizing activity was 1/11,785 and 1/6,036 (2). The comparable vaccine-elicited neutralizing antibody responses against HeV-g2 and HeV indicate that the changes in HeV-g2 G do not dampen polyclonal serum neutralizing activity.

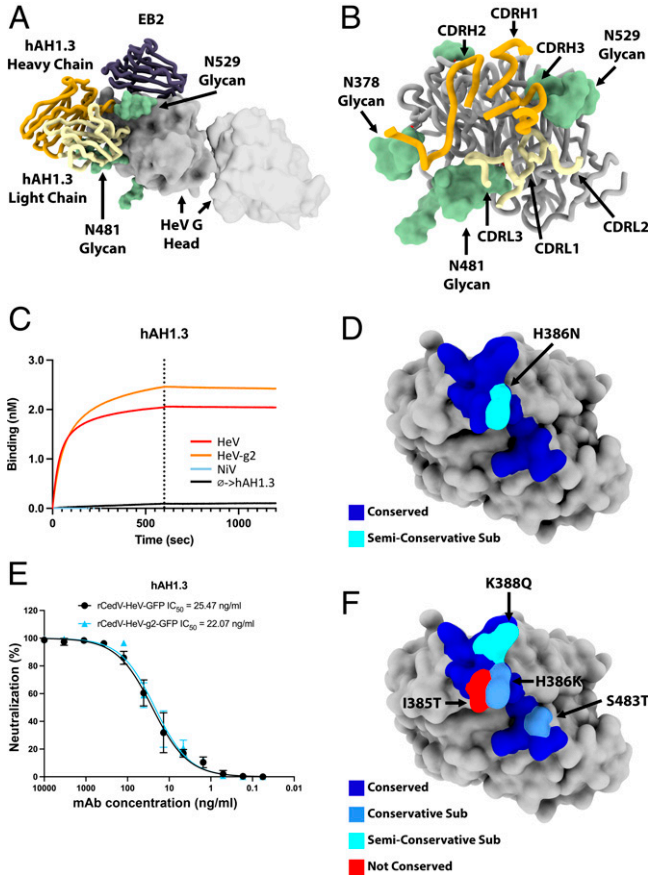

Fig. 4. hAH1.3 cross-reacts with and neutralizes HeV and HeV-g2. (*A*) Superimposition of the HeV G head domain (gray surface) bound to hAH1.3 (heavy and light chains are colored gold and yellow, respectively) with the EB2-bound NiV G head structure (purple; PDB ID code 2VSM; only EB2 is shown for clarity) showing the epitope does not overlap with the receptor binding site or the dimerization interface (transparent volume indicating the neighboring G head domain in the tetramer; PDB ID code 7TXZ). N-linked glycans are rendered as green surfaces. (*B*) Ribbon diagram of the HeV G head domain (gray) with the interacting hAH1.3 heavy- and light-chain CDRs rendered in gold and yellow, respectively. (*C*) BLI binding analysis of 100 nm hAH1.3 IgG to immobilized HeV G, HeV-g2, or NiV G head domains. (*D*) Molecular surface representation of the HeV G head showing the hAH1.3 footprint colored by residue conservation between HeV G and HeV-g2 G. Semi-Conservative sub, semiconservative substitution. (*E*) hAH1.3-mediated neutralization of rCedV-HeV-GFP (black) or rCedV-HeV-g2-GFP (blue). The limit of detection for the neutralization assay was 50 fluorescent foci. The hAH1.3 IC_{50} values were not statistically different (Student's *t* test) between rCedV-HeV-GFP and rCedV-HeV-g2-GFP ($P = 0.736$). Moreover, we observed a Pearson correlation of 0.9974 for the hAH1.3 IC_{50} values between rCedV-HeV-GFP and rCedV-HeV-g2-GFP with *P* values smaller than 0.0001. Error bars: SD. (*F*) Molecular surface representation of the HeV G head showing residue differences between HeV and NiV within the hAH1.3 epitope. Conservative sub, conservative substitution. Semi conservative sub, semi-conservative substitution.

Discussion

Since its discovery in 1994, 65 spillovers of HeV to domestic horses have been detected in Australia with sporadic human

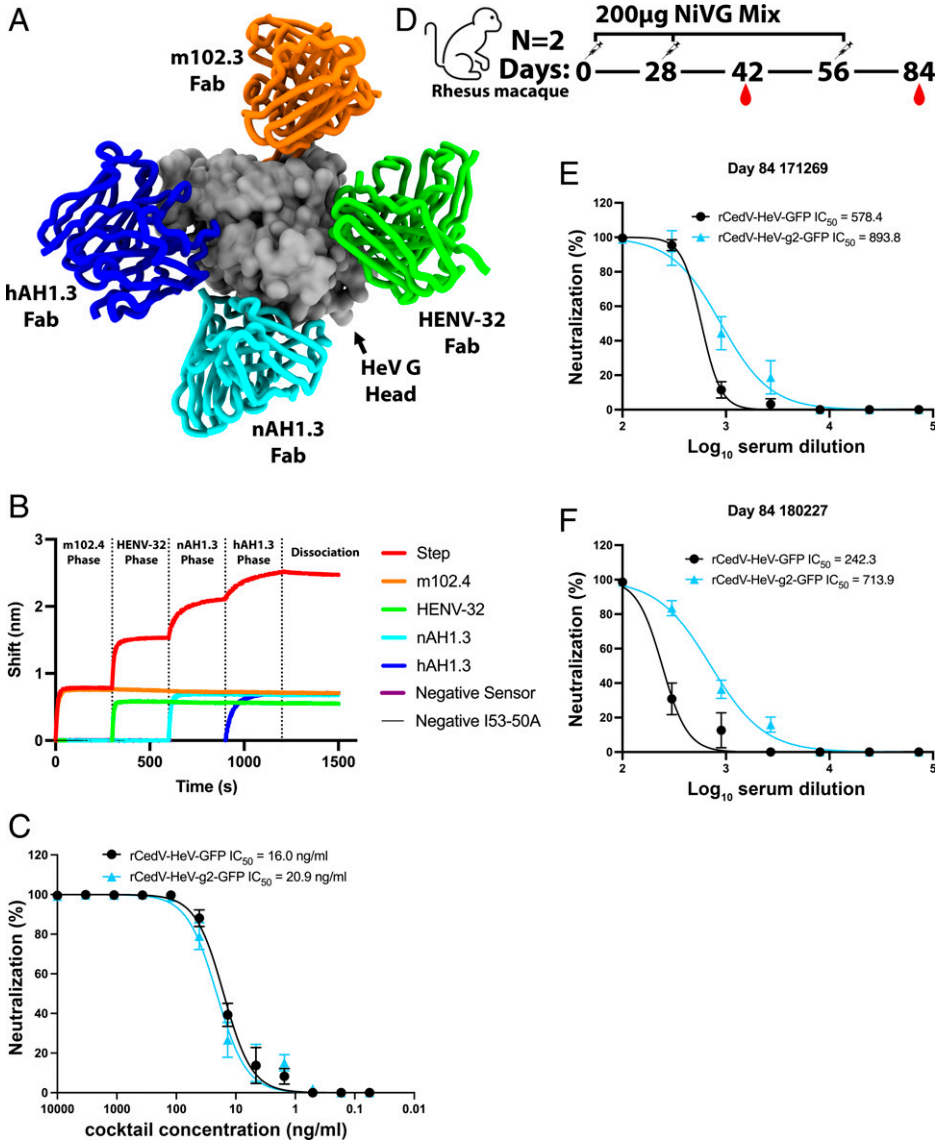

Fig. 5. G-targeted tetravalent mAb mixture and vaccine-elicited antibodies broadly neutralize HeV-g2. (*A*) hAH1.3 (blue), m102.3/m.102.4 (green), nAH1.3 (pink), and HENV-32 (red) mAbs recognize nonoverlapping epitopes on the HeV G head (gray). The HeV G head is rendered in the same orientation as in Fig. 4*A*, where the head–head dimerization interface faces to the right and the receptor-binding interface faces to the top. (*B*) BLI analysis of binding of m102.4, HENV-32, nAH1.3, and hAH1.3 IgG to the immobilized HeV G head showing the absence of competition among mAbs. The red trace shows the HeV G head-I53-50A fusion–loaded anti–penta-His biosensor sequentially dipped into a solution containing 100 nm m102.4, followed by 100 nm m102.4 + 100 nm HENV-32, followed by 100 nm m102.4 + 100 nm HENV-32 + 100 nm nAH1.3, followed by 100 nm m102.4 + 100 nm HENV-32 + 100 nm nAH1.3 + 100 nm hAH1.3, and buffer alone. Controls with only m102.4 IgG (orange), HENV-32 IgG (green), nAH1.3 IgG (cyan), and hAH1.3 IgG (blue) are shown for comparison. Negative sensor refers to an uncoated anti–penta-His biosensor dipped into 100 nm m102.4 + 100 nm HENV-32 + 100 nm nAH1.3 + 100 nm hAH1.3, and negative I53-50A refers to the HeV G head-I53-50A fusion–loaded anti–penta-His biosensor dipped into buffer alone. (*C*) Neutralization of rCedV-HeV-GFP (black) or rCedV-HeV-g2-GFP (blue) by the tetravalent m102.4/HENV-32/nAH1.3/hAH1.3 mAb mixture (1:1:1:1 molar ratio). (*D*) Study design for vaccination of rhesus macaques. Two animals were immunized three times (4 wk apart) with 200 µg of an alum-adjuvanted equimolar mixture of the purified NiV-B and NiV-M sG tetramers. Sera were collected on day 42 and day 84 postimmunization. (*E*) Day 84 NHP 171269 serum neutralizing activity against rCedV-HeV-GFP (black) and rCedV-HeV-g2-GFP (blue). (*F*) Day 84 NHP 180227 serum neutralizing activity against rCedV-HeV-GFP (black) and rCedV-HeV-g2-GFP (blue). The limit of detection for the neutralization assay was 50 fluorescent foci. Error bars: SD.

exposure and disease. A new HeV variant, termed HeV-g2, was recently described from two independent discoveries: one from a retrospectively diagnosed horse succumbing to henipaviral disease in 2015, which enabled a second fatal equine case to be diagnosed in October 2021, and the other from a long-term effort to monitor and survey the flying fox population in different states of Australia (26). The HeV-g2 genome differs from that of the prototypic HeV sufficiently to have failed detection by real-time RT-PCR–based disease surveillance in horses and viral reservoir surveillance of flying foxes. The identification of HeV-g2 extends the known HNV genetic diversity and also highlights the broad geographical range of potential HeV spillover.

We show here that HeV-g2 retains the same receptor tropism as prototypic HeV and utilizes EB2 and EB3 as bona fide entry receptors. Moreover, a panel of nine mAbs targeting several epitopes on the HeV F or G glycoprotein cross-reacts and retains potent neutralizing activities against HeV-g2. We describe a mAb, designated hAH1.3, cross-reacting with HeV and HeV-g2 G by targeting an antigenic site which is conserved among HeV variants but not NiV. As the epitopes of the hAH1.3, m102.4, HENV-32, and nAH1.3 neutralizing mAbs are distinct, we formulated a tetravalent mAb mixture potently neutralizing HeV and HeV-g2 which is expected to have a much higher barrier for the emergence of escape mutants

relative to individual constituting mAbs (2). Our data support the clinical development of multivalent mAb mixtures for post-exposure therapy as such countermeasures are expected to retain broad neutralizing activity against known and unknown NiV and HeV variants. NiV sG subunit vaccine-elicited neutralizing antibody responses are equivalently potent against HeV and HeV-g2, indicating that this newly emerged HeV-g2 variant does not erode cross-neutralizing polyclonal antibody responses more than HeV. We expect these findings to hold true in horses vaccinated with Equivac HeV and in humans, as the only HNV vaccine in clinical development is based on HeV sG which elicits better cross-protective titers than NiV sG against heterotypic challenge in animals (38). Collectively, our data provide a comprehensive assessment of available countermeasures against this newly described HeV-g2 variant and delineate multiple strategies for pandemic preparedness.

Materials and Methods

Constructs. The soluble ectodomain constructs of HeV F (whole genome from GenBank accession no. NC_001906.3; National Center for Biotechnology Information protein reference sequence NP_047111.2) and HeV-g2 F (GenBank accession no. UCY33669.1) were codon-optimized for a mammalian cell expression system, synthesized, and cloned into a pCDNA3.1+ vector by GenScript. These constructs include residues 1 to 487 followed by a GCNt trimerization domain and a C-terminal 8×His tag. Four point mutations (Y77C/G131C, N100C/A119C) were included to introduce two pairs of disulfide bonds known to stabilize HNV F in the prefusion conformation (12, 39).

The head domain constructs of HeV G (GenBank accession no. AAC83193.2) and HeV-g2 G (GenBank accession no. UCY33670.1) were codon-optimized for a mammalian cell expression system, synthesized, and cloned into a pCDNA3.1+ vector by GenScript. These constructs include residues 176 to 604 for HeV G and 175 to 603 for HeV-g2 G preceded by a 6×His tag and a GSGGGS linker at the N terminus.

The HeV G head domain construct used for the sequential BLI binding assay (HeV G head-I53-50A) includes the HeV head domain (residues 176 to 604) fused to the I53-50A component with a 16-GS linker in between and a GSGGGS linker with a 6×His tag at the very C terminus, where I53-50A has been described in Walls et al. (40).

The NiV G head domain includes residues 176 to 602 and introduces a linker (GSGGGS) between the 6×His tag and the head domain N terminus.

The *P. alecto* EB2 and EB3 Fc fusion constructs were codon-optimized for a mammalian cell expression system, synthesized, and cloned into a pCDNA3.1+ vector by GenScript. The human EB2 and EB3 Fc fusion constructs were codon-optimized for a mammalian cell expression system, synthesized, and cloned into a pTwist CMV vector by Twist Bioscience. These constructs include residues 1 to 229 for human EB2 (GenBank accession no. P52799), 28 to 224 for human EB3 (GenBank accession no. NP_001397), 28 to 224 for *P. alecto* EB2 (GenBank accession no. NP_001277099), and 29 to 226 for *P. alecto* EB3 (GenBank accession no. NP_001277094), followed by a linker (IEGRMD) and residues 100 to 330 of human IgG1 (GenBank accession no. P01857). For human EB2, the native signal peptide was therefore used. For human EB3 and *P. alecto* EB2 and EB3, MPMGSLQPLATLYLLGMLVASVLA was used as the signal peptide.

The nAH1.3 IgG construct was produced as previously described (2). HENV-32, HENV-103, and HENV-117 IgG genes were codon-optimized for a mammalian cell expression system, synthesized, and cloned into a pCDNA3.1+ vector by GenScript. The HENV-32 light-chain sequence was obtained from the Fab sequence of crystal structure Protein Data Bank (PDB) ID code 6VY4, and the HENV-32 heavy-chain sequence was reconstructed by combining the Fab sequence of crystal structure PDB ID code 6VY4 with a consensus sequence of IGHG1 (P01857). nAH1.3 and HENV-32 heavy chains include a StrepII tag (WSHPQFEK) linked by a linker sequence (GSGGGS) at the C terminus. HENV-103 and HENV-117 light- and heavy-chain constructs have been produced by replacing the variable domain of HENV-32 constructs with the corresponding HENV-103 or HENV-117 sequence. The C-terminal StrepII tag and linker have been removed for HENV-103 and HENV-117 heavy-chain constructs.

5B3, 1F5, 12B2, and hAH1.3 IgGs were produced from hybridomas and sequences are reported as sequenced.

All the constructs are listed in *SI Appendix*, Table S3.

Protein Expression and Purification. HNV glycoproteins were expressed in Expi293F cells by transient transfection using the ExpiFectamine 293 Transfection Kit (Thermo Fisher) according to the manufacturer's protocols. After 7 d in a humidified shaking incubator maintained at 37 °C and 8% CO_2, the transfected cells were harvested and cleared of cellular debris by centrifugation for 10 min at 1,000 × *g* followed by a hard spin for 30 min at 10,000 × *g*. The supernatants were then subjected to affinity chromatography.

His-tagged HeV F– or HeV-g2 F–containing supernatants were passed through a HisTrap FF affinity column (Cytiva) equilibrated in TBS (pH 8.0, 25 mM Tris, 150 mM NaCl). The column was then washed with 10 column volumes (CVs) of wash buffer (TBS, pH 8.0, 10 mM imidazole) and the protein was eluted in 10 CVs of elution buffer (TBS, pH 8.0, 500 mM imidazole). Proteins were subsequently concentrated and buffer-exchanged into TBS (pH 8.0) using 100-kDa cut-off Amicon centrifugal concentrators (EMD Millipore).

HeV, HeV-g2, and NiV G head domains as well as HeV G head-I53-50A were purified from clarified supernatants using a cobalt affinity column (Takara) equilibrated in phosphate buffered saline (PBS) (137 mM NaCl, 2.7 mM KCl, 10 mM Na_2HPO_4, and 1.8 mM KH_2PO_4, pH 7.4), and then washed by wash buffer (PBS, 10 mM imidazole), eluted by elution buffer (PBS, 500 mM imidazole), buffer-exchanged, concentrated, and flash-frozen in PBS.

nAH1.3, HENV-32, HENV-103, and HENV-117 IgGs and all ephrin Fc chimeras were purified from clarified supernatants using a 1-mL StrepTrap HP column (Cytiva) for nAH1.3 and HENV-32 and a 1-mL HiTrap Protein A HP column (Cytiva) for all ephrin Fc chimeras, buffer-exchanged, concentrated, and flash-frozen in PBS (137 mM NaCl, 2.7 mM KCl, 10 mM Na_2HPO_4, and 1.8 mM KH_2PO_4, pH 7.4). All columns were equilibrated in PBS (137 mM NaCl, 2.7 mM KCl, 10 mM Na_2HPO_4, and 1.8 mM KH_2PO_4, pH 7.4). The wash buffer used for all columns was PBS. The elution buffer for the StrepTrap HP column was PBS with 2.5 mM desthiobiotin, and for the HiTrap Protein A HP column was 0.1 M sodium citrate (pH 3.0); 1 M Tris (pH 8) was immediately added to the elution from the HiTrap Protein A HP column to neutralize the pH.

All proteins were flash-frozen and stored at −80 °C until further use.

HeV G and hAH1.3 Constructs Used for Structural Studies. The soluble head domain (amino acid residues 171 to 604) of HeV G was prepared as previously described (13). In brief, the construct was cloned into a pGP67 vector, with the GP67 signal peptide at the N terminus and no additional tag, and expressed in the Baculovirus Expression System (BD Biosciences). The conditional media of insect cell culture containing the HeV-G protein were purified using ion-exchange (Source 15Q and Mono Q columns, Cytiva) and size-exclusion chromatography (Superdex 200 column, Cytiva). For ion-exchange columns, we used 20 mM Tris·HCl (pH 8.0) as starting buffer, and then eluted using a gradient volume of 10 CVs with an increasing ionic strength up to 0.5 M NaCl. For the size-exclusion column, we used a buffer containing 20 mM Hepes (pH 7.2) and 10 mM NaCl. hAH1.3 IgG was purified from mouse hybridoma media with a protein A affinity column (31). Soluble hAH1.3 Fab was prepared by fragmentation of mouse hAH1.3 IgG using Pierce Mouse IgG1 Fab and F(ab')2 Preparation Kits according to the manufacturer's protocol. The HeV-G–hAH1.3 complex was obtained by mixing the two proteins in a 1:1.5 molar ratio and passed through a Superdex 200 column (Cytiva). The fractions containing both proteins were collected and concentrated to 10 mg/mL in a buffer containing 20 mM Hepes (pH 7.2) and 10 mM NaCl.

Expression of m102.4. m102.4 was isolated from a recombinant human phage-displayed Fab library and prepared as previously described (41). Briefly, CHO-K1 cells were transfected with a linearized m102.4 PDR12 construct and the antibody was purified with protein A from a selected stable m102.4-producing cell line (41). The human IgG1 m102.4 mAb has been extensively characterized as a highly potent HeV and NiV cross-reactive mAb (16, 17, 22, 25, 41, 42).

Generation of Fab Fragments from IgGs. The 1F5, 12B2, 5B3, and nAH1.3 Fabs were obtained by fragmentation of mouse IgGs using Pierce Mouse IgG1 Fab and F(ab')2 Preparation Kits according to the manufacturer's protocol.

BLI. Assays were performed on an Octet RED (ForteBio) instrument at 25 °C with shaking at 1,000 rpm. All proteins were diluted in kinetics buffer (KB) (Sartorius) to the desired concentration and loaded on appropriate biosensors at 10 to 20 μg/mL. All sensors were hydrated in water for 10 min prior to each experiment. F murine IgGs (1F5, 12B2, and 5B3) were loaded on anti-mouse Fc capture (AMC) biosensors. G human IgGs (m102.4 and HENV-32) and ephrin-Fc fusion proteins were loaded on anti-human Fc capture (AHC) biosensors, and G murine IgGs (nAH1.3 and hAH1.3) were loaded on AMC biosensors. HeV-g2 G head-I53-50A was loaded on anti–penta-His (HISK1) biosensors. All experiments were performed in technical replicates.

For kinetic measurements of F mAb (1F5, 5B3, and 12B2) binding to F proteins, trimeric HeV F or HeV-g2 F immobilized on Ni-NTA biosensors was dipped into solutions containing a threefold dilution series of Fab fragments at 300 to 1.23 nM.

For kinetic measurements of G mAb or ephrin-Fc fusion binding to G, mAbs or ephrin-Fc fusion proteins immobilized on AHC biosensors were dipped into various concentrations of HeV/HeV-g2 G head domain in KB in a threefold dilution series either from 30 to 0.124 nM or 3 μM to 12.4 nM.

All kinetics parameters and statistics were estimated from ForteBio software using a 1:1 binding model. Mean k_{on} and k_{off} values were determined with a global fit applied to all data.

For evaluation of hAH1.3 cross-reactivity, HeV, HeV-g2, or NiV G head domains immobilized on Ni-NTA biosensors were dipped into solutions containing 100 nM hAH1.3 IgG.

For competition binding assays using hAH1.3 and EB2, the HeV G head domain immobilized on Ni-NTA biosensors was dipped into solutions containing 100 nM hAH1.3 IgG and then 250 nM EB2 + 100 nM hAH1.3 IgG, or 100 nM hAH1.3 IgG only or 250 nM EB2 only.

For the tetravalent mAb mixture binding assays (m102.4, HENV-32, nAH1.3, and hAH1.3), HeV G head-I53-50A–loaded biosensors were dipped into 100 nM m102.4 in 10× KB, 100 nM m102.4 + 100 nM HENV-32, 100 nM m102.4 + 100 nM HENV-32 + 100 nM nAH1.3, 100 nM m102.4 + 100 nM HENV-32 + 100 nM nAH1.3 + 100 nM hAH1.3, and KB alone sequentially.

ELISA. Ninety-six-well MaxiSorp plates (Thermo Fisher) were coated overnight at 4 °C with 2 μg/mL nAH1.3, hAH1.3, m102.4, HENV-32, HENV-103, or HENV-117 IgG in 20 mM Tris and 150 mM NaCl (pH 8). Plates were slapped dry, washed three times in Tris-buffered saline Tween (TBST), and blocked with SuperBlock (Thermo Fisher) for 1 h at 37 °C. Plates were slapped dry and washed four times in TBST; 1:2 serial dilutions of either HeV or HeV-g2 G head domain (with initial concentration at 10 μM) were made in 50 μL TBST and incubated at 37 °C for 1 h. Plates were slapped dry and washed four times in TBST followed by addition of 50 μL 1:500 6×His tag monoclonal antibody (HIS.H8) horseradish peroxidase (HRP) (Thermo Fisher, MA1-21315-HRP) for 1 h at 37 °C. Plates were slapped dry and washed four times in TBST followed by addition of 50 μL TMB Microwell Peroxidase (SeraCare). The reaction was quenched after 4 min with 1 N HCl and the A_{450} of each well was read using a BioTek plate reader. Data were plotted and fit in Prism (GraphPad) using nonlinear regression sigmoidal, 4PL, X is log(concentration) to determine half-maximal effective concentration (EC_{50}) values from curve fits. All experiments were performed in technical triplicates.

Crystallization and Structure Determination of the HeV G Head Domain in Complex with hAH1.3 Fab. Crystallization of the HeV G head in complex with hAH1.3 was performed with a Mosquito robot (TTP LabTech). Initial hits were optimized with an additive screen (Hampton Research) using the sitting drop vapor diffusion method at room temperature. Ammonium sulfate as an additive was identified to improve crystal quality and related salts were subsequently screened. Final optimal crystals were obtained in conditions as follows: 22% (volume [vol]/vol) Tacsimate (pH 7.0), 0.1 M Hepes (pH 7.5), 0.1 M lithium sulfate, and 5% (vol/vol) polyethylene glycol 200. Crystals were frozen in liquid nitrogen with 25% glycerol as cryoprotectant. Diffraction data were collected at beamline NE-CAT ID-24 of the Advanced Photon Source at Argonne National Laboratory and were processed using the HKL2000 program (43). The structures were determined by molecular replacement with PDB ID code 3D11 (NiV-G) and a mouse Fab structural model was generated by SWISS-MODEL sequentially (44). Phaser, Coot, and phenix.refine in the program suite PHENIX were used for structure determination, model building, and refinement (45–47). The final model was validated using MolProbity and Privateer (48, 49). The details of the crystallographic analysis are presented in *SI Appendix*, Table S3.

Evaluation of Ephrin Receptor Tropism. HeLa-USU, HeLa-USU-EB2, and HeLa-USU-EB3 cells were seeded at a density of 2.5×10^5 cells per well in 12-well plates. The next day, cells were either uninfected (mock) or infected with rCedV-HeV-g2-GFP or rCedV-HeV-GFP at a multiplicity of infection of 0.5. At 24 h postinfection, rCedV-HeV-GFP– and rCedV-HeV-g2-GFP–infected cell cultures were monitored and imaged for GFP fluorescence. Images were captured with a Zeiss Axio Observer A1 inverted microscope using a 5× objective.

Fluorescence Reduction Neutralization Assay. Recombinant CedV chimeras were rescued and handled following laboratory manipulation guidelines and standard operating procedures under BSL-2 conditions that were developed, reviewed, and approved by the Uniformed Services University, Institutional Biosafety Committee in accordance with NIH guidelines (28, 50). A replication-competent rCedV chimera displaying the G and F proteins of HeV, and encoding GFP, was previously described (24). An rCedV chimera displaying the G and F proteins of HeV-g2, and encoding GFP, was similarly prepared here. mAbs were serially diluted threefold in Dulbecco's modified Eagle's medium containing 10% v/v fetal bovin serum to final concentrations ranging from 10 μg/mL to 0.05 ng/mL. For the mAb mixture neutralization assay, each mAb was present at a quarter of the indicated concentrations. The diluted mAbs (individual or the mixture) were added 1:1 to a target of 2,000 plaque-forming units of either rCedV-HeV-g2-GFP or rCedV-HeV-GFP and incubated for 2 h at 37 °C. The virus/mAb mixture (90 μL) was then incubated with confluent Vero 76 cells in black-walled clear-bottom 96-well plates (Corning Life Sciences) at 37 °C. Following a 24-h incubation, cells were fixed with 4% formaldehyde in PBS for 20 min at room temperature. The cells were then gently washed four times with deionized water and scanned using the CTL S6 analyzer (Cellular Technology Limited). Fluorescent foci were counted using the CTL Basic Count feature and S6 software. Percent neutralization was calculated by normalizing counts to a virus-only control. The IC_{50} was determined as the mAb concentration at which there was a 50% reduction in fluorescent foci versus virus-only control wells. The data represent the average and SDs from two independent experiments each performed in duplicate and are plotted as a nonlinear regression curve fit with variable slope using GraphPad Prism. The IC_{50} or half maximal inhibition dilution (ID_{50}) values were calculated from a nonlinear fit model using GraphPad Prism. The limit of detection for this assay was 50 fluorescent foci. Statistical analysis was performed by Student's *t* test. A Pearson correlation analysis was performed with the neutralization values obtained by FRNT with each mAb against the rCedV-HeV-GFP and rCedV-HeV-g2-GFP chimeras, and there was a very strong correlation with the percent neutralization values between rCedV-HeV-GFP and rCedV-HeV-g2-GFP chimeras ($r \geq 0.9$ with $P < 0.0001$).

Data Availability. The hAH1.3-bound HeV G head structure has been deposited to the Protein Data Bank with accession number PDB 7SYY. All study data are included in the article and/or *SI Appendix*.

ACKNOWLEDGMENTS. This study was supported by the National Institute of Allergy and Infectious Diseases (Grants DP1AI158186 and HHSN272201700059C to D.V.; Grant AI142764 to C.C.B. and D.V.), a Pew Biomedical Scholars Award (to D.V.), Investigators in the Pathogenesis of Infectious Disease Awards from the Burroughs Wellcome Fund (to D.V.), the University of Washington Arnold and Mabel Beckman cryoelectron microscopy center, and NIH Grant S10OD032290 (to D.V.). D.V. is an Investigator of the Howard Hughes Medical Institute. E.J.A. and the "Horses as Sentinels" research were supported by the Australian Government Department of Agriculture, Water and the Environment, Biosecurity Innovation Program (Project ID 202043). We thank Auro Vaccines, LLC, for providing the rhesus macaque NiV-M and NiV-B sG immune sera, and also acknowledge the Coalition for Epidemic Preparedness Innovations for their support of the Nipah virus vaccine program. Molecular graphics and analyses were performed with UCSF ChimeraX, developed by the Resource for Biocomputing, Visualization, and Informatics at the University of California, San Francisco (UCSF), with support from NIH Grant R01-GM129325 and the Office of Cyber Infrastructure and Computational Biology, National Institute of Allergy and Infectious Diseases. The opinions and assertions expressed herein are those of the authors and do not necessarily reflect the official

policy or position of the Uniformed Services University or the Department of Defense, or the Henry M. Jackson Foundation for the Advancement of Military Medicine, Inc. Additional support was provided by the Ohio State University Comprehensive Cancer Center, and Path to K Grant GR125041 through the Ohio State University Center for Clinical & Translational Science (to K.X.).

Author affiliations: [a]Department of Biochemistry, University of Washington, Seattle, WA 98195; [b]Department of Microbiology and Immunology, Uniformed Services University, Bethesda, MD 20814; [c]Henry M. Jackson Foundation for the Advancement of Military Medicine, Bethesda, MD 20814; [d]Department of Veterinary Biosciences, The Ohio State University, Columbus, OH 43210; [e]US Public Health Services Commissioned Corps, Rockville, MD 20852; [f]Sydney School of Veterinary Science, University of Sydney, Sydney, 2570 NSW, Australia; [g]Sydney Institute for Infectious Diseases, University of Sydney, Sydney, 2006 NSW, Australia; [h]Black Mountain Laboratories, Health and Biosecurity, Commonwealth Scientific and Industrial Research Organisation, Canberra, 2601 ACT, Australia; [i]Equine Veterinary and One Health Epidemiology, EquiEpiVet, Aireys Inlet, Surf Coast, 3231 VIC, Australia; [j]University of Sydney School of Medicine, Sydney, 2006 NSW, Australia; [k]Westmead Institute for Medical Research, Sydney, 2145 NSW, Australia; [l]Private Equine Veterinary Practice, Brisbane, 4034 QLD, Australia; and [m]HHMI, University of Washington, Seattle, WA 98195

Author contributions: Z.W., H.V.D., M.A., K.X., C.C.B., and D.V. designed research; Z.W., H.V.D., M.A., Y.X., R.Y., L.Y., A.C.H., and K.X. performed research; E.J.A., B.A.H., P.A.R., I.S., and J.-S.E. contributed new reagents/analytic tools; Z.W., H.V.D., M.A., K.X., C.C.B., and D.V. analyzed data; and Z.W., H.V.D., C.C.B., and D.V. wrote the paper.

Competing interest statement: C.C.B. is a US federal employee and coinventor on US and foreign patents pertaining to soluble forms of Nipah virus and Hendra virus G glycoproteins. C.C.B. and M.A. are coinventors on US and foreign patents pertaining to Cedar virus and methods of use and recombinant Cedar virus chimeras, whose assignee is the United States as represented by the Henry M. Jackson Foundation for the Advancement of Military Medicine.

1. B. T. Eaton, C. C. Broder, D. Middleton, L.-F. Wang, Hendra and Nipah viruses: Different and dangerous. *Nat. Rev. Microbiol.* **4**, 23–35 (2006).
2. Z. Wang *et al.*, Architecture and antigenicity of the Nipah virus attachment glycoprotein. *Science* **375**, 1373–1378 (2022).
3. J. J. W. Wong *et al.*, Monomeric ephrinB2 binding induces allosteric changes in Nipah virus G that precede its full activation. *Nat. Commun.* **8**, 781 (2017).
4. K. Xu *et al.*, Host cell recognition by the Henipaviruses: Crystal structures of the Nipah G attachment glycoprotein and its complex with ephrin-B3. *Proc. Natl. Acad. Sci. U.S.A.* **105**, 9953–9958 (2008).
5. O. A. Negrete *et al.*, EphrinB2 is the entry receptor for Nipah virus, an emergent deadly paramyxovirus. *Nature* **436**, 401–405 (2005).
6. T. A. Bowden *et al.*, Structural basis of Nipah and Hendra virus attachment to their cell-surface receptor ephrin-B2. *Nat. Struct. Mol. Biol.* **15**, 567–572 (2008).
7. M. I. Bonaparte *et al.*, Ephrin-B2 ligand is a functional receptor for Hendra virus and Nipah virus. *Proc. Natl. Acad. Sci. U.S.A.* **102**, 10652–10657 (2005).
8. K. Xu *et al.*, Crystal structure of the pre-fusion Nipah virus fusion glycoprotein reveals a novel hexamer-of-trimers assembly. *PLoS Pathog.* **11**, e1005322 (2015).
9. C. T. Pager, W. W. Craft Jr., J. Patch, R. E. Dutch, A mature and fusogenic form of the Nipah virus fusion protein requires proteolytic processing by cathepsin L. *Virology* **346**, 251–257 (2006).
10. C. T. Pager, R. E. Dutch, Cathepsin L is involved in proteolytic processing of the Hendra virus fusion protein. *J. Virol.* **79**, 12714–12720 (2005).
11. H. V. Dang *et al.*, Broadly neutralizing antibody cocktails targeting Nipah virus and Hendra virus fusion glycoproteins. *Nat. Struct. Mol. Biol.* **28**, 426–434 (2021).
12. H. V. Dang *et al.*, An antibody against the F glycoprotein inhibits Nipah and Hendra virus infections. *Nat. Struct. Mol. Biol.* **26**, 980–987 (2019).
13. K. Xu *et al.*, Crystal structure of the Hendra virus attachment G glycoprotein bound to a potent cross-reactive neutralizing human monoclonal antibody. *PLoS Pathog.* **9**, e1003684 (2013).
14. V. A. Avanzato *et al.*, A structural basis for antibody-mediated neutralization of Nipah virus reveals a site of vulnerability at the fusion glycoprotein apex. *Proc. Natl. Acad. Sci. U.S.A.* **116**, 25057–25067 (2019).
15. K. N. Bossart *et al.*, A Hendra virus G glycoprotein subunit vaccine protects African green monkeys from Nipah virus challenge. *Sci. Transl. Med.* **4**, 146ra107 (2012).
16. K. N. Bossart *et al.*, A neutralizing human monoclonal antibody protects against lethal disease in a new ferret model of acute Nipah virus infection. *PLoS Pathog.* **5**, e1000642 (2009).
17. T. W. Geisbert *et al.*, Therapeutic treatment of Nipah virus infection in nonhuman primates with a neutralizing human monoclonal antibody. *Sci. Transl. Med.* **6**, 242ra82 (2014).
18. C. E. Mire *et al.*, A cross-reactive humanized monoclonal antibody targeting fusion glycoprotein function protects ferrets against lethal Nipah virus and Hendra virus infection. *J. Infect. Dis.* **221**, S471–S479 (2019).
19. M. Amaya, C. C. Broder, Vaccines to emerging viruses: Nipah and Hendra. *Annu. Rev. Virol.* **7**, 447–473 (2020).
20. D. Middleton *et al.*, Hendra virus vaccine, a One Health approach to protecting horse, human, and environmental health. *Emerg. Infect. Dis.* **20**, 372–379 (2014).
21. T. W. Geisbert *et al.*, A single dose investigational subunit vaccine for human use against Nipah virus and Hendra virus. *NPJ Vaccines* **6**, 23 (2021).
22. K. N. Bossart *et al.*, A neutralizing human monoclonal antibody protects African green monkeys from Hendra virus challenge. *Sci. Transl. Med.* **3**, 105ra103 (2011).
23. J. Dong *et al.*, Potent Henipavirus neutralization by antibodies recognizing diverse sites on Hendra and Nipah virus receptor binding protein. *Cell* **183**, 1536–1550.e17 (2020).
24. M. P. Doyle *et al.*, Cooperativity mediated by rationally selected combinations of human monoclonal antibodies targeting the Henipavirus receptor binding protein. *Cell Rep.* **36**, 109628 (2021).
25. E. G. Playford *et al.*, Safety, tolerability, pharmacokinetics, and immunogenicity of a human monoclonal antibody targeting the G glycoprotein of Henipaviruses in healthy adults: A first-in-human, randomised, controlled, phase 1 study. *Lancet Infect. Dis.* **20**, 445–454 (2020).
26. J. Wang *et al.*, A new Hendra virus genotype found in Australian flying foxes. *Virol. J.* **18**, 197 (2021).
27. E. J. Annand *et al.*, Novel Hendra virus variant detected by sentinel surveillance of horses in Australia. *Emerg. Infect. Dis.* **28**, 693–704 (2022).
28. E. D. Laing *et al.*, Rescue and characterization of recombinant Cedar virus, a non-pathogenic Henipavirus species. *Virol. J.* **15**, 56 (2018).
29. K. N. Bossart *et al.*, Functional studies of host-specific ephrin-B ligands as Henipavirus receptors. *Virology* **372**, 357–371 (2008).
30. G. A. Marsh *et al.*, Cedar virus: A novel Henipavirus isolated from Australian bats. *PLoS Pathog.* **8**, e1002836 (2012).
31. V. Borisevich *et al.*, Escape from monoclonal antibody neutralization affects Henipavirus fitness in vitro and in vivo. *J. Infect. Dis.* **213**, 448–455 (2016).
32. A. C. Walls *et al.*, Unexpected receptor functional mimicry elucidates activation of coronavirus fusion. *Cell* **176**, 1026–1039.e15 (2019).
33. L. Piccoli *et al.*, Mapping neutralizing and immunodominant sites on the SARS-CoV-2 spike receptor-binding domain by structure-guided high-resolution serology. *Cell* **183**, 1024–1042.e21 (2020).
34. F. A. Lempp *et al.*, Lectins enhance SARS-CoV-2 infection and influence neutralizing antibodies. *Nature* **598**, 342–347 (2021).
35. T. N. Starr *et al.*, SARS-CoV-2 RBD antibodies that maximize breadth and resistance to escape. *Nature* **597**, 97–102 (2021).
36. M. A. Tortorici *et al.*, Broad sarbecovirus neutralization by a human monoclonal antibody. *Nature* **597**, 103–108 (2021).
37. M. A. Tortorici *et al.*, Ultrapotent human antibodies protect against SARS-CoV-2 challenge via multiple mechanisms. *Science* **370**, 950–957 (2020).
38. B. A. Mungall *et al.*, Feline model of acute Nipah virus infection and protection with a soluble glycoprotein-based subunit vaccine. *J. Virol.* **80**, 12293–12302 (2006).
39. J. J. W. Wong, R. G. Paterson, R. A. Lamb, T. S. Jardetzky, Structure and stabilization of the Hendra virus F glycoprotein in its prefusion form. *Proc. Natl. Acad. Sci. U.S.A.* **113**, 1056–1061 (2016).
40. A. C. Walls *et al.*, Elicitation of potent neutralizing antibody responses by designed protein nanoparticle vaccines for SARS-CoV-2. *Cell* **183**, 1367–1382.e17 (2020).
41. Z. Zhu *et al.*, Exceptionally potent cross-reactive neutralization of Nipah and Hendra viruses by a human monoclonal antibody. *J. Infect. Dis.* **197**, 846–853 (2008).
42. A. Di Rubbo *et al.*, Optimization and diagnostic evaluation of monoclonal antibody-based blocking ELISA formats for detection of neutralizing antibodies to Hendra virus in mammalian sera. *J. Virol. Methods* **274**, 113731 (2019).
43. Z. Otwinowski, W. Minor, Processing of X-ray diffraction data collected in oscillation mode. *Methods Enzymol.* **276**, 307–326 (1997).
44. A. Waterhouse *et al.*, SWISS-MODEL: Homology modelling of protein structures and complexes. *Nucleic Acids Res.* **46**, W296–W303 (2018).
45. A. J. McCoy *et al.*, Phaser crystallographic software. *J. Appl. Crystallogr.* **40**, 658–674 (2007).
46. P. Emsley, B. Lohkamp, W. G. Scott, K. Cowtan, Features and development of Coot. *Acta Crystallogr. D Biol. Crystallogr.* **66**, 486–501 (2010).
47. P. V. Afonine *et al.*, Towards automated crystallographic structure refinement with phenix.refine. *Acta Crystallogr. D Biol. Crystallogr.* **68**, 352–367 (2012).
48. C. J. Williams *et al.*, MolProbity: More and better reference data for improved all-atom structure validation. *Protein Sci.* **27**, 293–315 (2018).
49. J. Agirre *et al.*, Privateer: Software for the conformational validation of carbohydrate structures. *Nat. Struct. Mol. Biol.* **22**, 833–834 (2015).
50. E. D. Laing *et al.*, Structural and functional analyses reveal promiscuous and species specific use of ephrin receptors by Cedar virus. *Proc. Natl. Acad. Sci. U.S.A.* **116**, 20707–20715 (2019).